Facile synthesis of chitin nanocrystal decorated on 3D cellulose aerogel as a new multi-functional material for waste water treatment with enhanced anti-bacterial and anti-oxidant properties

Gopi, Sreerag; Balakrishnan, Preetha; Divya, Chandradhara; Valić, Srećko; Govorčin Bajsić, Emi; Pius, Anitha; Thomas, Sabu

Source / Izvornik: **New journal of chemistry, 2017, 41, 12746 - 12755**

Journal article, Accepted version
Rad u časopisu, Završna verzija rukopisa prihvaćena za objavljivanje (postprint)

https://doi.org/10.1039/C7NJ02392H

Permanent link / Trajna poveznica: https://urn.nsk.hr/urn:nbn:hr:184:748909

NJC

Accepted Manuscript

This article can be cited before page numbers have been issued, to do this please use: S. Gopi, P. Balakrishnan, C. Divya, S. Valic, E. Govorcin Bajsic, A. Pius and S. Thomas, *New J. Chem.*, 2017, DOI: 10.1039/C7NJ02392H.

ROYAL SOCIETY OF CHEMISTRY

rsc.li/njc

View Article Online
DOI: 10.1039/C7NJ02392H

Facile synthesis of chitin nanocrystal decorated on 3D cellulose aerogel as a new multi-functional material for waste water treatment with enhanced anti-bacterial and anti-oxidant properties

Sreerag Gopi [a, b, c], *Preetha Balakrishnan* [b, c], *Chandradhara Divya* [d], *Srecko Valic* [e], *Emi Govorcin Bajsic*[f], *Anitha Pius* [*, a], *Sabu Thomas* [*, b, c]

[a]Department of Chemistry, Gandhigram Rural Institute - Deemed University, Gandhigram, Dindigul District – 624302, Tamilnadu, India.
[b]School of Chemical Sciences, Mahatma Gandhi University, Kottayam–686560, Kerala, India.
[c]International and Inter University Centre for Nanoscience and Nanotechnology, Mahatma Gandhi University, Kottayam – 686560, Kerala, India.
[d]Bio-Agile Therapeutics Private Limited, Niran Arcade, 563/564, Ground floor, New Bel road, Bangalore 560094, Karnataka, India

[e]Center for Micro and Nano Sciences and Technologies, Radmile Matejčić 2, 51000 Rijeka, Croatia, and Rudjer Bošković Institute, Bijenička c. 54, 10000 Zagreb, Croatia

[f]Faculty of Chemical Engineering and Technology, Marulićev trg 19, 10000 Zagreb, Croatia

Keywords: Aerogels, Cellulose, Chitin, Hybrid bio-aerogels, Anti-bacterial

Corresponding authors:
Prof. (Dr.) Anitha Pius
Email:dranithapius@gmail.com
Ph: +91-9443108504 (Mob.),
+91-4512452371 (Off.)

Prof. (Dr.) Sabu Thomas
Email: sabuthomas@mgu.ac.in
Ph: +91-9447223452

Abstract

We report fabrication and application of multi-functional hybrid bio-aerogels based on cellulose nanofibers (CNF)and chitin nano crystals (CNC)developed through environmental friendly freeze-drying process. Herein, organic non-solvent approach such as acid hydrolysis was used to extract CNF and CNCfrom corn husk and shrimp shell respectivelyfollowed bycharacterisationusing IR spectroscopy and electron microscopy. Usual wired like and infrequent semi-square type of morphology were detected for CNF and CNCrespectivelyduring electron microscopic analysis. The aerogels with two different quantities of CNC on CNFwere

View Article Online
DOI: 10.1039/C7NJ02392H

made (AR1 and AR2) and compared them with reference to the neat CNF aerogel (neat AR). Interestingly, for AR2, under the electron microscopy, a maple seed like morphology was observed compared to neat AR and AR1.Their ability in water treatmentwere determinedby conducting adsorption experimentusing methylene blueand Rhodamine 6G, found that AR2 has enhanced removal percentage and adsorption capacity. To addressing their economic viability, we conducted several rounds of studies and evaluated the reusability of AR2. Anti-bacterial and anti-oxidant activities of aerogels were studied using disc diffusion method against four bacterial species such as St. aureus, E. coli, S. typhimurium and B. Cereus and carefully discussed the best condition for the determination of minimal inhibitory concentration. The prepared material having higher CNC content (AR2) shows multi-functional behaviour and in the future further studies are anticipated to produce them in industrial scale for commercial application

1. Introduction

Government, industries, and customers are gradually demanding products developed from sustainable and renewable resources that are biodegradable, carbon neutral, non-petroleum, and have low environmental, human or animal health and safety risks. For the past thousand years natural, cellulose based materials have been used by our society as engineering materials and their use continues in paper production and in textile field world widely. Cellulose is a linear polysaccharidewhich contains glucose molecules in a ringed and flat ribbon like conformation. The repeating unit of cellulose comprised of two anhydroglucose rings $(C_6H_{10}O_5)_n$; n= 10000 to 15000, where n is depended on the cellulose source material linked together through an oxygen covalently to C1 of one glucose ring and C4 of adjoining ring (1→4 linkage) and so called the β 1→4 glucosidic bond[1]. Cellulose mainly occurs as microfibrilated form having both amorphous and crystalline regions. The isolation of crystalline region and dissolution of amorphous region

View Article Online
DOI: 10.1039/C7NJ02392H

makes cellulose into nanocrystals usually known as cellulose nanofibrilshaving similar properties of raw one. The low mechanical stability and charge less surface is main disadvantage of cellulose and cellulose nanofiber which can be overcome using reinforcement of other substances during the material processing time.Another polysaccharide known as chitin is a natural, renewable and biodegradable polymer, the second most abundant biopolymer after cellulose[2]which can be found in exoskeleton shells of arthropods such as crabs, shrimps, beetles etc and cell walls of fungi and yeasts[3–5]. Chitin also a linear polysaccharide containing repeated units of β-(1→4)-2-acetamido-2-deoxy-β-D-glucose and β-(1→4)-2-amino-2-deoxy-β-D-glucose[6]. Chitin has two hydroxyl groups and an acetamide group makes chitin very crystalline with surface charge and strong hydrogen bonding[7]. Similar to cellulose, chitin also occurs in nature as microfibrilated form having both amorphous and crystalline regions and these fibrils are typically embedded in a protein matrix depending on the origin of sources[8]. The crystalline regions of chitin can be extracted by excluding amorphous region and it is known as chitin nanocrystals or nanowhiskerswhich is widely used as reinforcing nanoparticles. Several methods can be employed for the extraction of chitin nanocrystals such as acid hydrolysis[8–17], mechanical treatment[7,18], electrospinning[19], gelation[20], and TEMPO-mediated oxidation[21,22]. Due to the diverse properties of chitin nanocrystals such as biodegradability, functionality, hydrophilicity, eco-friendly, and ease of processing, it is used in many field of application which includes biomedical, water purification, packing and protein immobilization[23]. Recently Lin et. al reported fungus – derived chitin nanocrystals and their dispersion stability evaluation in aqueous media. In their study, chitin nanocrystals which avoided possible safety risks were extracted from mushrooms using protein/mineral purification and HCl hydrolysis. Such nanocrystals of

View Article Online
DOI: 10.1039/C7NJ02392H

chitin's were in α-crystalline structure with a length and width of 143 ± 24 and 10 ± 2 nm respectively[24].

Water pollution from industrial as well as public effluents (dyes, heavy metals, oils etc) results in acute shortage of fresh water in many parts of the world in which dyes and heavy metals can severely damage people and living things[25]. Consequently there is an increasing demand for advancedadsorptive materials having high selectivity, high efficiency and high adsorption capacity[25,26]. The dye effluents are one of major contaminants in water. Different types of adsorptive materials including activated carbon[27], carbon nanotubes[28], clays[29], magnetic oxides[30]etc are being used for the adsorption of dyes from waste water. Among them, 3D porous materials seem to be the most auspicious class of high performance adsorbent due to their high porosity, light weight and large surface to volume ratio. Because of these inherent physio-chemical characteristics, they can adsorb a large quantity of dye molecules from dye polluted waste water according to their surface charges. However, complex fabrication procedures and/or high raw materialcost have diminished their wide spread applicability. Therefore, there is every need to develop innovative, renewable/sustainable, eco-friendly and robust high performance adsorbent materials.

Xiong et.al demonstrated a facile and environmentally friendly approach to prepare $F_{e3}O_4$/Ag nanofibrillated cellulose nanocomposite aerogel having excellent catalytic properties for the reduction of 4-nitophenol. This prepared aerogels also showed high antibacterial activity against model microbe *S. aureus*[31]. Zhou et. al prepared polyaniline (PANI) – decorated cellulose aerogel with strong interfacial adhesion and enhanced photocatalytic activity via dissolve/regeneration route using ionic liquid[32].In this study, cellulose nanofibril-chitin nanocrystal hybrid aerogel have been developed for the first time using environmentally friendly

View Article Online
DOI: 10.1039/C7NJ02392H

freeze drying process[33]. Theirapplication in dye waste water treatment, anti-bacterial and anti-oxidant properties were evaluated very carefully. Cellulose is the richest natural, renewable, biodegradable and biocompatible polymer in the world[34]. Cellulose nanofibrils have high aspect ratios and high surface areas, hence they certainly form an entangled web like structure[35,36]. Cellulose nanofibers can be prepared using different methods including 2, 2, 6, 6-tetramethylpiperidine-1-oxyl (TEMPO)-mediated oxidation[36,37], mechanical shearing[38], and high-pressure homogenization[39,40]. The aerogels made from cellulose nanofiber usually show high surface areas, reasonable mechanical, thermal properties and also low densities[41–43]. They have been used in a variety of applications, such as thermal insulation[34], anti-bacterial agent[44] and oil absorbents[45,46]. Chitin nanocrystals is an economical polymer which contains desired properties such as water solubility, compatibility and functionality. New hybrid aerogel structures based on chitin nanocrystal and cellulose nanofiber having an innovative maple seed type morphology have been made use of for the first time for the macromolecular engineering of new class of aerogels which is an excellent advanced bio-based green materialfor dye adsorption from aqueous solution. Interestingly, the acetamide groups in chitin nanocrystal control anti-bacterial properties of aerogels.

2. Experimental Section

2.1.Materials

The cellulose extracted from local dried corn husk has been used in the present study. The chitin used for producing the chitin nanocrystal, was a commercially supplied fully bleached shrimp shell flakes. Sulfuric acid,sodium hypochlorite solution, methylene blue(MB), rhodamine 6G (Rh) and other chemicals were obtained from sigma Aldrich.They were used without further

View Article Online
DOI: 10.1039/C7NJ02392H

purification. Millipore-MilliQ distilled water was employed during the complete experiments. Table 1 shows the specification of dyes used in this study.

Table 1. Specifications of MB and Rh

Generic name	**Methylene blue**
Color Index Number	52015
Molecular formula	$C_{16}H_{18}ClN_3S$
Molecular weight	319.85
I_{max} (nm)	609
Generic name	**Rhodamine 6G**
Color Index Number	45160
Molecular formula	$C_{28}H_{31}N_2O_3Cl$
Molecular weight	479.01
I_{max} (nm)	530

2.2.Preparation of Cellulose Nanofibers

Cellulose nanofiber (CNF) prepared from corn husk were collected from the local area, Slovenia and thoroughly washed with running tap water followed by soaked in Millipore-MilliQ water later dried under sunlight. The washed corn husk was bleached (treated) with aqueous sodium chlorite (1.7 wt % $NaClO_2$in water). The bleaching treatment was performed at 90 ^oC for 2h followed by acetic acid was added to reach pH 4 to enhance the bleaching reaction. The resultant fibers were repeatedly washed in distilled water until the pH became neutral and later dried at 60 ^oC for 12 h in an air circulating oven.The nanofibers were prepared from treated corn fibers by following already reported method of Khawas et.al[47]with suitable modifications. In brief, the methodology is as follows: the dried corn fibers were crushed and treated with sodium hydroxide solution (4 %) at boiling condition for 2 h under thorough stirring to solubilize lignin, pectin and hemicelluloses. This step was done at least 3 times for complete purification of the fibers. The resulting fibers were hydrolyzed with 65 % (w/w) sulfuric acid for about 60 min

View Article Online
DOI: 10.1039/C7NJ02392H

using mechanical stirrer to dissolute the amorphous region and to isolate the required nanofibers. Subsequently, the suspension was diluted with ice cubes to quench the reaction followed by washing and centrifuging at 10000 rpm for 20 min. The CNF suspension was homogenized by using PRIMIX-Homomixer homogenizer for 15 min and stored in refrigerator.

2.3.Preparation of Chitin Nanocrystals

Chitin nanocrystal (CNC) were prepared by following the study reported by Gopi et al.[48]with suitable modifications. The powdered shrimp shells were suspended in 5 % aqueous potassium hydroxide solution for 6 h under boiling condition in order to remove the proteins and minerals from it. The obtained residue was rinsed with distilled water, filtered and kept for agitation at room temperature followed by bleaching with 17 g of sodium hypochlorite solution for 2 h at 80^{o}C. The resulting dispersion was hydrolyzed with sulfuric acid, filtered and washed with three times and CNC solution transferred into dialysis bag. The dialysis was continued until the pH of CNC solution reached 6 followed by ultrasonicated for 5 min. The CNC solution was stored in refrigerator to prevent from bacterial growth.

2.4.Preparation of Cellulose Nanofiber/Chitin nanocrystal hybrid aerogels

The Cellulose Nanofiber/Chitin nanocrystal hybrid aerogels (CNC/CNF) were fabricated by a cost effective environmental friendly freeze-drying method. 6 and 12.5 mL of 1mg mL^{-1} CNC aqueous dispersion were mixed with 50 mL of 1.2 wt% CNF to get the final concentrations of 1 % and 2 % and named as AR1 and AR2 respectively.The resulting mixture was sonicated using a probe sonicator for 10 min to overcome the agglomerates and finally casted in petridishes. Neat CNF aerogel (neat AR) without the addition of CNC was made as a reference. The whole solutions were precooled in a 3 ^{o}C refrigerator to avoid macroscopic fracture during

View Article Online
DOI: 10.1039/C7NJ02392H

the freezing step. Later the precooled samples were frozen at -73 ^{o}C in a dry ice- iso-propanol solution and freeze dried in a lyophilizer at a condenser temperature of -88.0 ^{o}C under vacuum for 4 days to fabricate aerogels. Finally, the samples of aerogel were stored in vacuum oven for further characterization.

2.5.Fourier transform infrared spectroscopy

Fourier transform infrared spectroscopy (FTIR) analysis was used to detect the chemical moieties present in CNF, CNC and CNF/CNC hybrid aerogel recorded using Shimadzu IR-470 IR spectrophotometer. The FTIR spectra for every samples were attained over the wavelength ranging from 400 to 4000 cm^{-1} using potassium bromide disk and the experiments were carried out with a resolution of 2 cm^{-1}.

2.6. X-ray diffraction analysis

X-ray diffraction analysis was employed to determine the crystalline nature of CNF and CNC. The powdered materials of CNF and CNC were placed in the sample holder and leveled to get uniform and total X-ray exposure. The X-ray diffraction patterns of CNF and CNC achieved with as X-ray diffractometer (Bruker Diffractometer D8 Advanced Model) at room temperature with 2Θ from 5 to 60 ^{o} and with scan rate of 2 ^{o} min^{-1}

2.7. Transmission electron microscopy

Transmission electron microscopy ((TEM) JEOL-2100 model) was used to determine the morphology and dimension of CNF and CNC. Prior to TEM analysis diluted suspension of CNF and CNC pasted on a copper grid and dried at room temperature. The analysis was carried out with accelerating voltage of 25 KV.

View Article Online
DOI: 10.1039/C7NJ02392H

2.8. Field emission scanning electron microscopy

The morphology of CNF/CNC hybrid aerogel was observed using field emission scanning electron microscopy ((FESEM (JEOL JSM-820 Model))with operation voltage of 20 kV. All samples were dried at 40 ^{o}C and coated with vanadium to avoid following charging before SEM observation.

2.9. BET analysis

Nitrogen adsorption-desorption isotherms were measured using a Quantachrome® ASiQwin™, and Brunauer – Emmet – Teller (BET) and Barret – Joyner – Halenda (BJH) analysis were obtained using the Autosorb software (Quantachrome®). The BET analysis was performed at relative vapor pressures of 0.08 – 0.3 (P/P_0) and the BJH analysis was done from desorption isotherm branch. The pore-size distribution and surface area were calculated using BJH and BET methods.

2.10. Swelling studies

Circularly shaped samples with diameter ≈ 2 cm of ASTM standard D5890 were weighed and immersed in toluene contained in test tubes with airtight stoppers kept at room temperature for 72 h. Afterwards the initial weight, swollen weight and deswollen weight were taken using a high sensitive electronic balance device. Cross link densities of the aerogel samples were calculated from swelling experiments using Flory-Rehner equation.

2.11.Thermal gravimetric analysis

Thermal gravimetric analysis (TGA) was conducted for CNF/CNC hybrid aerogels by using Perkin Elmer Pyris 1 thermogravimetric system under nitrogen purge, with a flow rate 100 mL

View Article Online
DOI: 10.1039/C7NJ02392H

min^{-1}. The scanning rate was 10 ^{o}C min^{-1} and the temperature ranging from 40 to 700 ^{o}C. All samples were left at 40 ^{o}C for 3 min before the measurements to avoid the moisture.

2.12. Differential scanning calorimetry

Thermal properties of CNF/CNC aerogels were studied by differential scanning calorimetry (DSC) with DSC instrument Mettler Toledo 822^{e} using nitrogen atmosphere. The DSC stands as a thermal technique by which I and II order of polymer materials phase transitions can be easily determined. About 9-11 mg of samples were heated to 200^{o}C from room temperature and stands isothermally for 15 min to exclude the effect of the thermal history during sample processing. Subsequently, the samples were cooled and reheated to 200^{o}C. Experiments were carried out with heating/cooling rate of 10 ^{o}C min^{-1}. The phase transition temperatures were determined from the second DSC cycle.

2.13. Performance of Cellulose nanofiber/Chitin nanocrystal hybrid aerogel on waste water treatment

The dye removal studies of aerogels were carried out using methylene blue (MB) and Rhodamine 6G (Rh 6G). 1000 mgL^{-1} dye concentration in water was used as stock solution. From the stock solution, dilutions of 10 mgL^{-1} concentrations of dyes were made and kept at neutral pH. All the analysis was demonstrated at room temperature with the help of UV-VIS spectrophotometer (Agilent technologies, Cary 60 UV-VIS). The samples (1 cm^2) hanged into a glass chamber with a magnetic stirrer and 250 mL of dye solution transferred into it. The adsorption of MB and Rh 6G were measured at the absorbance maxima λ_{max} = 609 nm and λ_{max} = 530 nm respectively. The percentage of removal of MB and Rh 6G with different adsorbents were calculated by following eq. (1)[49];

View Article Online
DOI: 10.1039/C7NJ02392H

$$R = \frac{C_i - C_0}{C_i} \cdot 100\ \% \quad (1)$$

where C_i (mgL^{-1}) is the initial concentration of solution and C_0 (mgL^{-1}) is the final concentration of solution.

The following eq. (2) was used for calculating the dye adsorption capacity of the adsorbents:[49]

$$q_e = \frac{(C_i - C_0)V}{m} \quad (2)$$

where q_e is expressed in mg/g, V is the volume of solution and m is the mass of adsorbent.

2.14. Antimicrobial and antioxidant activity studies of Cellulose nanofiber/Chitin nanocrystal hybrid aerogel

Four bacterial species were employed as test organisms which include *Staphylococcus aureus, Escherichia coli, Salmonella typhimurium, Bacillus cereus*. The bacteria were maintained in Mueller – Hinton (MH). Inoculate were prepared by adding an overnight culture of the organism in MH broth to obtain an OD600 0.1. The cells were allowed to grow until they obtain the McFarland standared 0.5 (approximately 108 CFU/mL). The suspension was then diluted to 1: 1000 in MH broth to obtain 106 CFU/mL. The antibacterial and antioxidant activities were carried out using neat AR, AR1 and AR2.

3. Results and discussions

3.1.Fourier transform infrared spectroscopy

The fourier transform infrared (FTIR) spectroscopy was used to analysis the chemical moieties present in CNF, CNC, neat AR and AR2 shown in the figure 1. The FTIR spectra of CNF and neat AR show a broad peak at a frequency of 3300 cm^{-1} which corresponds to polysaccharide

View Article Online
DOI: 10.1039/C7NJ02392H

hydroxyl group. The peaks at 2900-2800 cm^{-1} represent the C-H symmetrical stretching vibrations. The FTIR spectrum of CNC in which, peaks at 1663 cm^{-1}, 1630 cm^{-1} correspond to amide I and peak at 1556 cm^{-1} corresponds to amide II bands. These are typical well characterized peaks for chitin alredy reported in the scientific literature[15]. Peak at 3451 cm^{-1} represents -OH group and peak at 3259 cm^{-1} attributed to -NH group. The FTIR spectrum of AR2 having 2 wt.% of CNC shows the same peaks as of CNF or neat AR and also along with the peaks of CNC such as 1663 cm^{-1}, 1630 cm^{-1} and 1556 cm^{-1}which correspond to amide I and amide II bands respectively. AR2 also shows peak at 3259 cm^{-1} attributed to -NH group. To the better understanding about the interaction between CNC over neat AR, FTIR spectra of the same were compared.One thing can be observed that neat AR have a well-defined single peak around 3300 cm^{-1} corresponds to -OH functionality. But in AR2, the peak multiplies and a combined multiple peak of both -OH (3300 cm^{-1}) and amide group (3259 cm^{-1})observed which possibly due to the hydrogen bonding interaction between the CNF and CNC. Compared to neat AR, AR2 have new peaks at 1663 cm^{-1}, 1630 cm^{-1} correspond to amide I and peak at 1556 cm^{-1} corresponds to amide II bands of CNC which were absent in AR. This confirms better interaction and nanoscale reinforcement of CNC over AR2. The similar observation has been reported by Sun et.al in chitosan (chitin)/cellulose composite biosorbents prepared using ionic liquid for heavy metal ions adsorption. They reported that hydroxyl stretching vibrations for chitosan (chitin) and cellulose located at 3436 cm^{-1} and 3343 cm^{-1} were broadened and shifted to 3413 cm^{-1} indicated that stronger intermolecular hydrogen bonds interaction[50].From the demonstrated FTIR spectra of neat and nanocomposites hybrid aerogel it can be confirmed the presence of CNC in AR2 and the reinforcement doesn't make any changes in chemical moieties present in CNF based aerogel.

View Article Online
DOI: 10.1039/C7NJ02392H

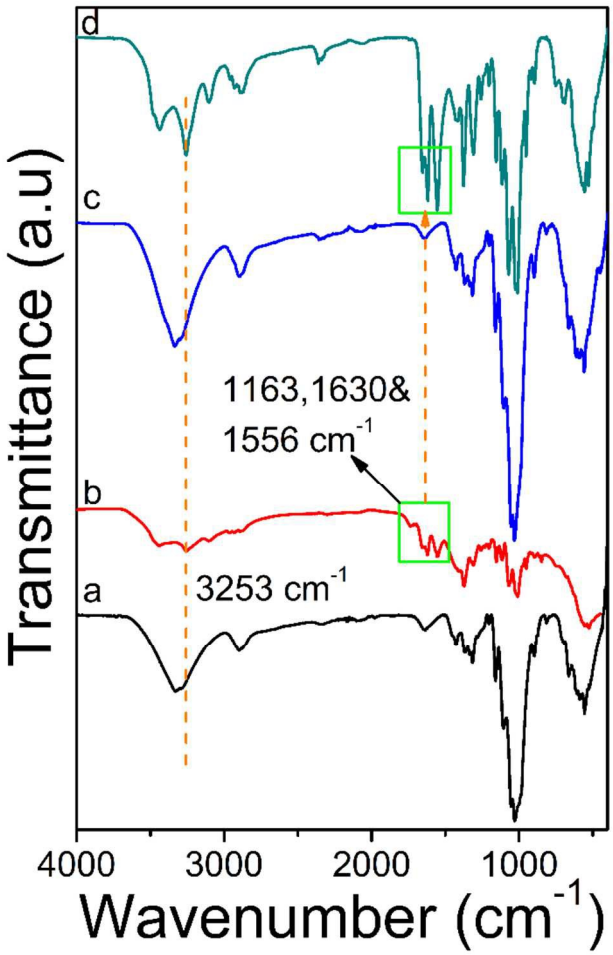

Figure 1. FTIR spectra of a) CNF, b) CNC, c) neat AR and d) AR2.

3.2. X-ray diffraction (XRD) analysis

X-ray diffraction (XRD) analysis were employed to reveal crystallinity of CNF and CNC shown in figure 2. The XRD profile of CNF have two major peaks corresponds to $2\Theta = 16.1^{o}$ and 22.8^{o} which is characteristically structure of cellulose I and sharp peak at 22.8^{o} is due to higher crystallinity of cellulose. In the case of CNC, two major diffraction peaks at $2\Theta = 9.8^{o}$ and 19.5^{o} along with three minor peaks at 12.6^{o}, 23.9^{o}, and 26.8^{o} were observed. In CNC, the high crystalline nature and structure is due to the van der Waals and hydrogen bonding interaction in it.

View Article Online
DOI: 10.1039/C7NJ02392H

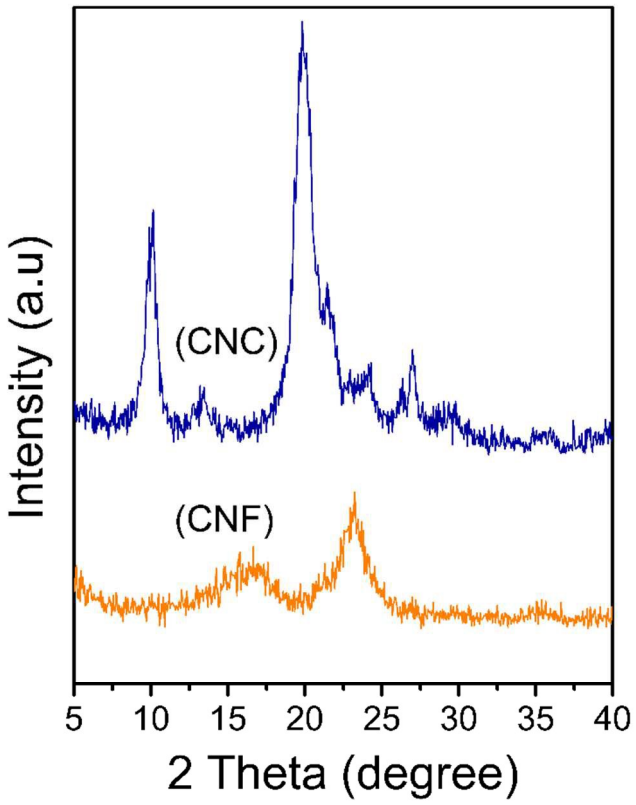

Figure 2. XRD spectra of CNF and CNC

3.2. Transmission electron microscopy

The transmission electron microscopy (TEM) images and size distribution graphs of both CNF and CNC in different resolutions given in figure 3. Let us examine the TEM images of CNF which is shown in figure 3 a. Uniform suspension of CNF was achieved after mild acid hydrolysis of purified corn husk which is shown in the insight of figure 3 a. A wire like morphology can be observed for CNF with slight agglomeration which may due to the insufficient ultra-sonic treatment. Agglomeration also could be possible due to the water evaporation from the CNF suspension during the sample preparation.The average diameter from the size distribution graph was found to be in the range of 60-120 nm.Similar CNF morphology were reported by Asha et. al[51] in their studies.

View Article Online
DOI: 10.1039/C7NJ02392H

Let us now examine the TEM images of CNC. The CNC isolated from shrimp shell using sulfuric acid hydrolysis shows a different morphology compared to other reported studies. The TEM image of CNC show a needle type or rod like structure in most of the reported studies[15,52]. In our present study, CNC shows semi-square crystal morphology which is shown in the figure 3. The crystalline nature and morphology of the product depends on the raw materials and chemical treatment process. An inconsiderable agglomeration also can be observed from the TEM images of CNC which can influence dispersion behavior on CNF suspension. We also observed bright crystalline nature of powdered CNC (achieved by lyophilizing) by visually, which is shown the inset of figure 3 b. The average size from the size distribution graph was found to be in the range of 20-100 nm.

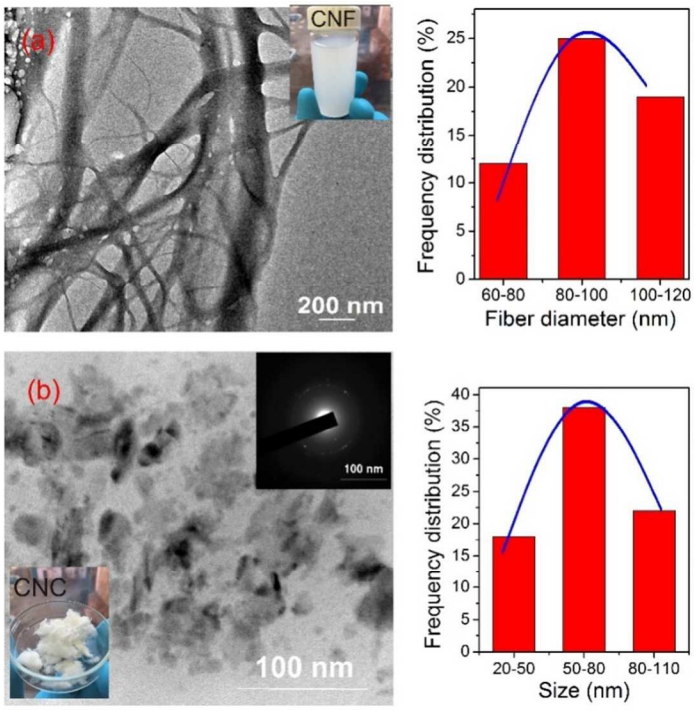

Figure 3. TEM images of a) CNF, b) CNC and their size distribution diagrams.

3.3. Field emission scanning electron microscopy

View Article Online
DOI: 10.1039/C7NJ02392H

The morphologies under different resolutions of neat aerogel, AR1 and AR2 were observed and analysed using field emission scanning electron microscopy (FESEM) as shown figure 4. The images of neat AR show random, non-oriented porous structure having distribution in size and these pores were large in size. The fibers were not well interconnected and aggregation of fibers also can be observed. Nanofibers have a tendency to attract each other and this could be a reason for the above-mentioned aggregations. While the images of AR1 show, smaller pores compared to neat AR due to the small addition of CNC which may influence the morphological behaviour of CNF aerogel. In the other case, the images of AR2 containing higher amount of CNC show a notable morphological behaviour compared to neat AR and AR1. The morphological character of AR2 can be compared with layer-by-layer of maple seed. From a clear observation, it can be understood thata single maple seed contains a well oriented vein, these veins interlocked between each other and also a rough texture on the surface. The FESEM images of AR2 is very similar to multi-layer maple seed type morphology demonstrated here. The fiber orientation in AR2 is also mimicking the maple seed which clearly observed from the FESEM image of the same. Upon higher amount of CNC reinforcement, ithas a tendency to locate in between CNF that reduces the intermolecular interaction between the fibers. Consequently, it hinders the chances of aggregation resulting to obtain fiber networking leading to branch like maple seed morphology. This type of morphology is expected to have potential applications in various fields such as water treatment (adsorption, filtration), drug delivery, tissue engineering etc.

View Article Online
DOI: 10.1039/C7NJ02392H

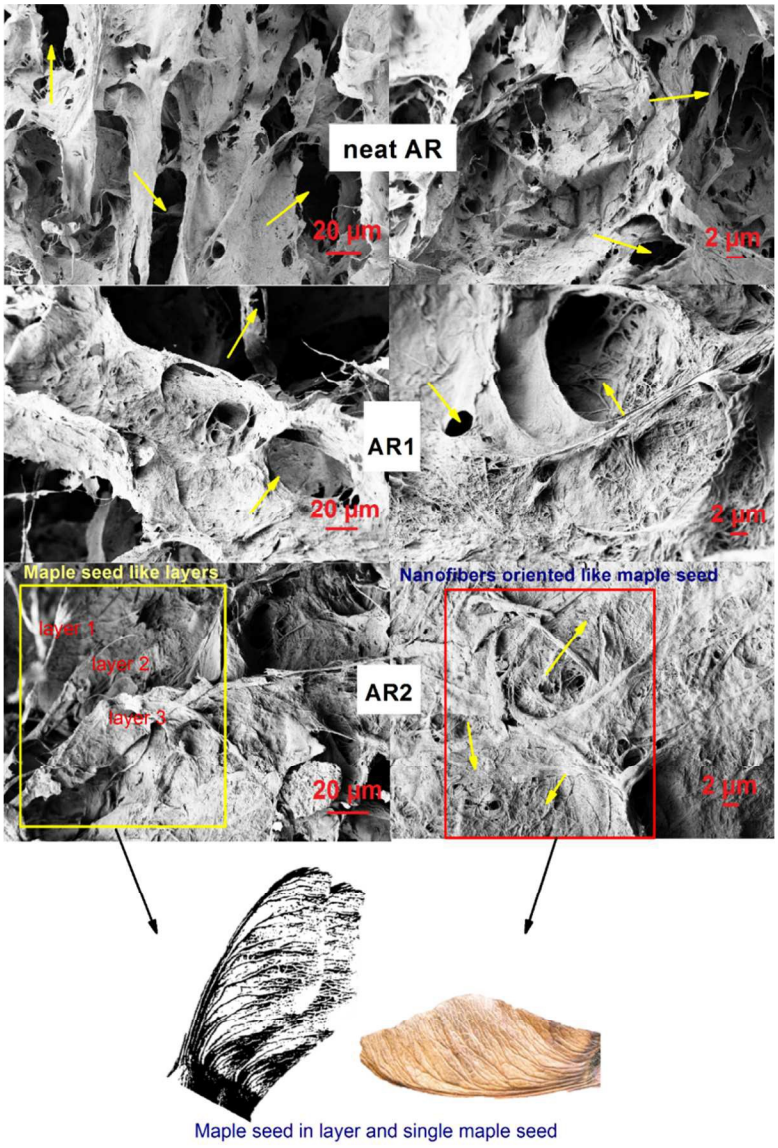

Figure 4. FESEM images of aerogels

3.4. BET analysis

BET surface area, pore diameter and pore volume of neat AR, AR1 and AR2 given in table 2. It can be observed that the pore volume is decreasing gradually from neat AR (0.24 cc/g) with an increasing in levels of CNC content. AR2 has lesser pore volume (0.029 cc/g) compared to AR1 (0.039 cc/g) since higher level of CNC content in AR2 significantly changes the pore structure. A decrease in pore diameter can also be observed from neat AR to AR1 and then AR2,

View Article Online
DOI: 10.1039/C7NJ02392H

this arises by filling the pores of AR2 with the higher CNC compared to AR1. BET surface area value of AR2 was 17.508 nm which is higher than AR1 and neat AR, this increase in surface area can improve the efficiency of adsorption performance.

Table 2. Specifications of MB and Rh

Aerogels	Pore volume (cc/g)	Pore diameter (nm)	BET surface area (m^2/g)
Neat AR	0.24	1.595	11.473
AR1	0.036	1.564	13.608
AR2	0.029	1.555	17.508

3.5. Cross-link density studies

According to the theory of swelling behavior of cross-linked polymers, strong bonding such as chemical cross link between the cellulose nanofiber and chitin nanocrystal chains prevent the molecules from completely surrounded by the fluids, but they can cause swelling. The percentage of increase in swollen mass was calculated by the following equation.

$$Swollen\ mass\ increase\ (\%) = [(m_1 - m_0)/m_0] \times 100 \quad (3)$$

where m_0 initial weight of the sample and m_1 is weight of sample after immersing into the solvent in which the solvent specimens cleared by using filter paper.

Cross-link density is usually calculated from equilibrium swelling data by means of the Flory-Rehner equation[53–55].

$$\text{Cross-link density } V = 1/2\, M_c \quad (4)$$

$$M_c = \left[-\rho_r V_s V_{rf}^{1/3}\right]/\left[\ln\left(1 - V_{rf}\right) + V_{rf} + \chi V_{rf}^2\right] \quad (5)$$

$$V_{rf} = [(d - fw)\rho_r]/[([(d - fw)\rho_r]) + (A_s/\rho_s)] \quad (6)$$

View Article Online
DOI: 10.1039/C7NJ02392H

where M_c is the molecular weight of polymer between cross-links, $\rho_r$is the density of polymer, V_s and V_{rf} are molar volume of the solvent and volume fraction of the polymer in the swollen sample respectively. In which d represent deswollen weight f is the volume fraction of filler, w is the initial weight of the material, A_s is the adsorbed amount of solvent by the material. The interaction parameter χ, shown in eqn (4) and is given by Hildebrand equation

$$\chi = \beta + \left[V_s(\rho_s - \rho_\rho)^2/RT\right] \quad (7)$$

here β is the lattice constant, R represent the universal gas constant, T is absolute temperature, ρ_s and $\rho_\rho$are the solubility parameter of solvent and solubility parameter of the polymer respectively. Table 1 shows the cross-link density values obtained by swelling experiments. Aerogel containing higher amount of CNC (AR2) exhibit higher cross-link density value except AR1 such as $V = 0.420 \times 10^4$ (mol cm^{-3}) and $V = 3.4124 \times 10^4$ (mol cm^{-3}) for AR1 and AR2 respectively. The functional groups (hydroxyl and acetamide groups) of CNC on cellulose nanofiber can act as a network forming agents able to react with the CNF chains leading to the formation of strong networking structure in the aerogel.

3.6. Thermal gravimetric analysis

The thermal gravimetric analysis (TGA) curves for AR1 and AR2 in comparison with reference neat AR are shown in figure 5. All materials show decrease in mass at 100^{o}C which obviously due to the evaporation of adhering moisture from the materials. By careful evaluation of obtained data, we can observe that AR2 losses only 5.2 % of mass at this temperature which is low compared to other reported studies[56,57]. This may due to the freeze-drying process that sublimate the whole water moieties from the sample. Also, the mass loss of AR2 at 100 ^{o}C lower than neat AR and AR1 (8.4 % and 7.8 % respectively) probably due to fine dispersion of CNC

View Article Online
DOI: 10.1039/C7NJ02392H

on CNF thus leaving no vacant space for entrapment of water molecules. The AR2 with relatively higher CNC content unveiled an onset weight loss at around 290 ^{o}C, which was higher than neat AR and AR1 having lower CNC content. The TGA results showed that thermal stability of AR2 aerogel was the best among all the samples (neat AR and AR1). This suggested that there existstrong interaction between CNF and CNC in AR2.

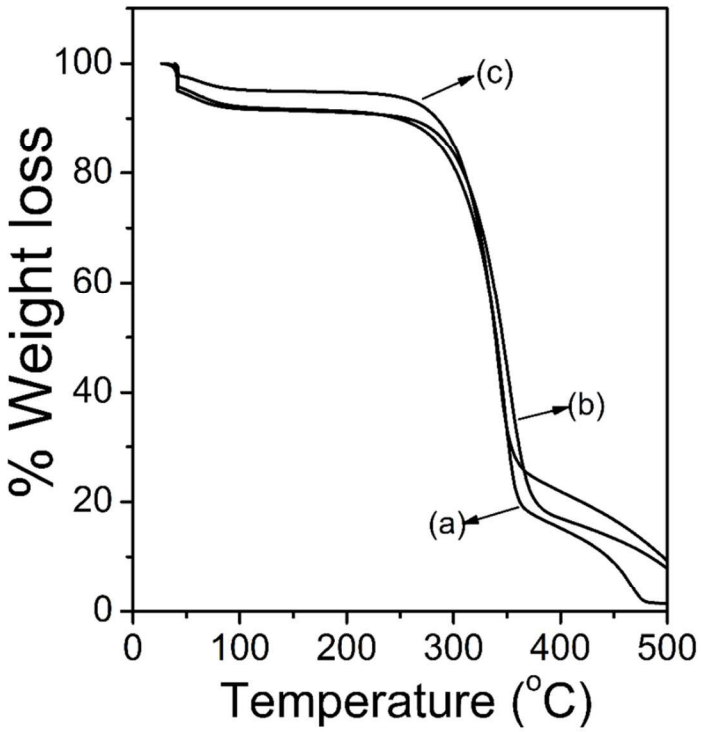

Figure 5. TGA curves of a) neat AR, b) AR1 and c) AR2.

3.7. Differential scanning calorimetry

The differential scanning calorimetry (DSC) curves of neat AR, AR1 and AR2 are shown in figure 6 a. It can be seen that the melting temperatures (T_m) of neat AR and AR1 (104.9^{O}C)are much lower than AR2 (126.6^{O}C). The high melting temperature of AR2 is due to the uniform dispersion of CNC in CNF as mentioned in morphological part, which prevents the motion of CNF chains. As a result, more energy is needed for the molecular motion of CNF chains. The

View Article Online
DOI: 10.1039/C7NJ02392H

more is the crystalline region, the higher will be the melting temperature. A graphical representation given in figure 6 b showing better organization and alignment of nanofibers in AR2 having higher amount of CNC that can be leads to higher crystallinity and melting point.

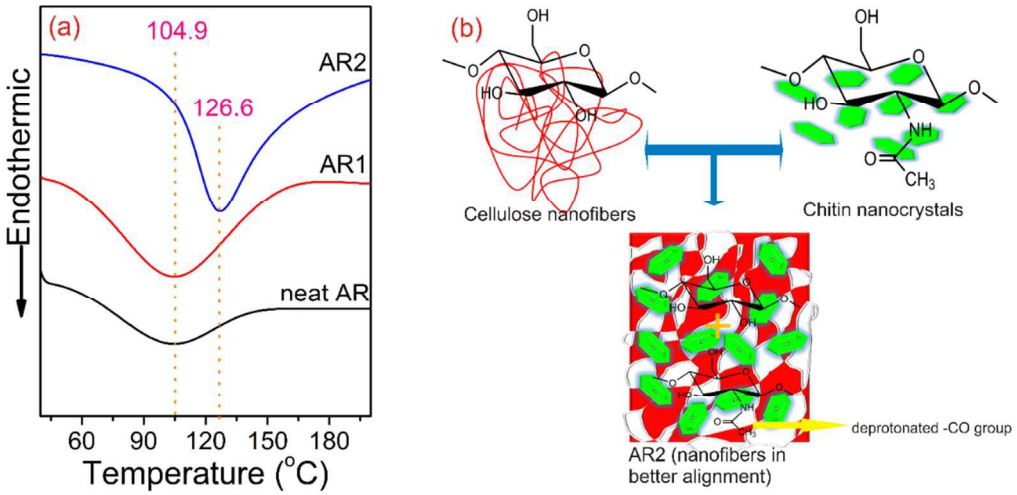

Figure 6a) DSC curve of aerogels b) Graphical representation of aligned fibers in AR2

3.8. Performance of Cellulose nanofiber/Chitin nanocrystal hybrid aerogel on waste water treatment

The effect of contact time on the dye water treatment using MB and Rh are shown in figure 7. It is clearly observed that the percentage of removal (removal (%)) and adsorption capacity (q_e) of neat AR and AR1 are low compared to AR2. The percentage of removal and adsorption capacity of AR2 were found to be 80.07 % and 8 mg/g for MB, 92.89 % and 9.2 mg/g for Rh respectively. A schematic representation of mechanism of MB and Rh adsorption onto AR2 is shown figure 8. The AR2 material contains higher amount well dispersed CNC on CNF and the CNCs are enriched with acetamide groups. During the course of adsorption, the deprotonated carbonyl group present in acetamide (reactive group in CNC) creates a negative charge species as shown in the scheme (inside the green one). These negatively charged CNChas

View Article Online
DOI: 10.1039/C7NJ02392H

an electrostatic interaction between positively charged dye molecule which is shown as doted lines. These electrostatic interactions favour efficient dye adsorption over the CNC decorated AR2. It is also important to consider the well-designed morphological texture in AR2 as already discussed under morphological part which could be anotherpossibility of the enhanced dye removal from water.

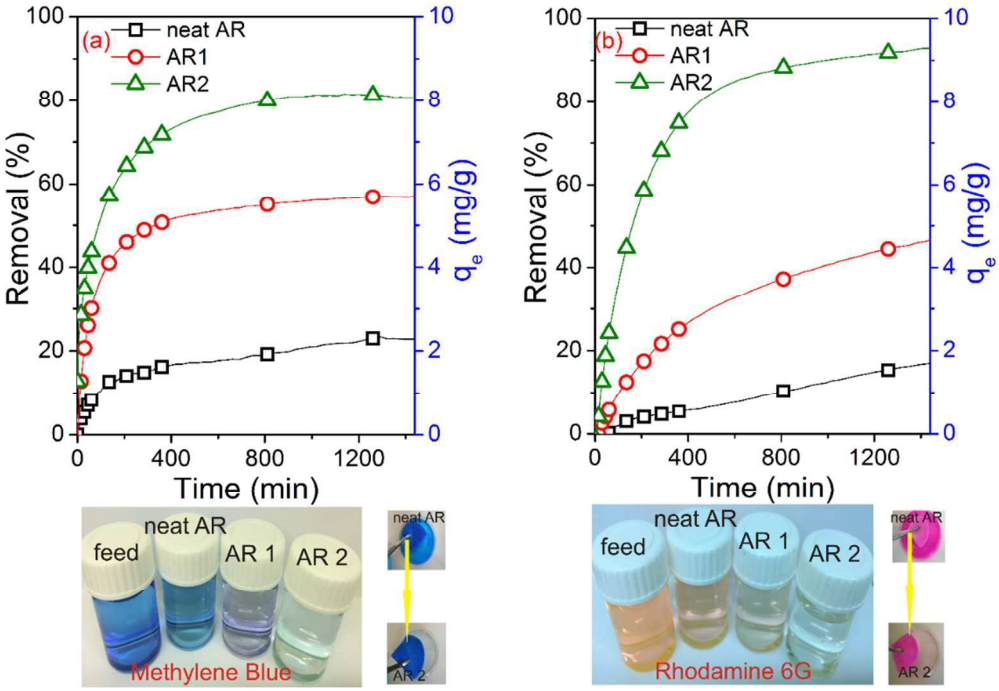

Figure 7. Removal(R) and adsorption capacity (q_e) of neat AR, AR1 and AR2 on a) MB and b) Rh.

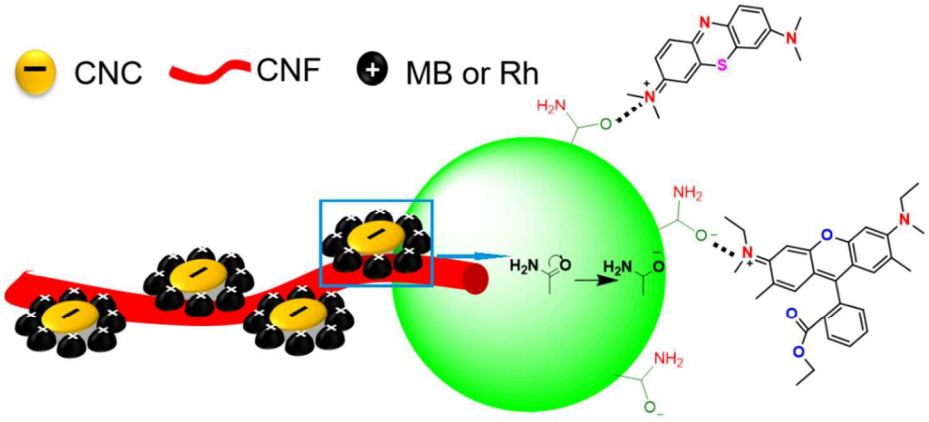

View Article Online
DOI: 10.1039/C7NJ02392H

Figure 8. Schematic representation of mechanism of MB and Rh adsorption onto AR2.

3.9. Round studies of material

Round studies were carried out using AR2 on MB and Rh to understand the reusability of material. After the first-round of adsorption experiment the sample AR2 was dried at room temperature and washed several times using distilled water. Totally 5round experiments were conducted with the same drying and washing protocols and the results are shown in figure 9. During the first round, 80.07 % MB and 92.87 % Rhcould be removedand the removal efficiency was gradually found decreased and in the final round i.e. in 5thround 30.2 % MB and 52.9 % Rh could be removed using AR2. The decreasing efficiency up reuse could be explained as follows: During the several adsorptions process the active sites of material were occupied with dye molecule and few of them only could be removed during thoroughwashing procedure[58]. As a result, subsequent adsorption process, active sites required to adsorb dye molecules reduces. Thereby a reduction in adsorption takes place in the round studies. Even though AR2 can be reused by simple washing and drying process in several times, one has to sacrifice the efficiency.

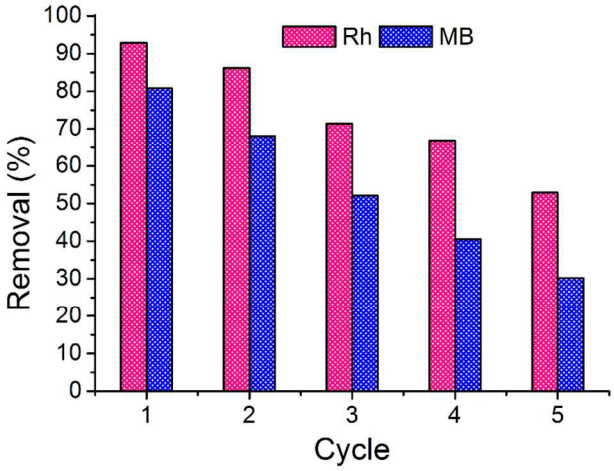

Figure 9. Reusability of AR2 on removal of Rh and MB

View Article Online
DOI: 10.1039/C7NJ02392H

3.10. Antimicrobial and antioxidant activity studies of Cellulose nanofiber/Chitin nanocrystal hybrid aerogel

Determination of antibacterial activity. The discs such as neat AR, AR1 and AR2 were placed on Mueller-Hinton agar plates, previously swabbed with the target bacterial isolate at a concentration of 106 CFU/mL. In one disc, the respective organic solvent was added as negative control to determine possible inhibitory activity of the solvent. This preparation was incubated for a period of 24 h at 30 ^{o}C. Antibacterial activity was defined as the diameter of the clear inhibitory zone formed around the discs. The MIC of the extract was determined by tube dilution technique in Mueller-Hinton broth (supplied by Merck) according to NCCLS. The range of concentration used was 156.25 to 5000 µg/mL. The four last vials of each bacterium with no growth from the MIC procedure were streaked onto nutrient agar (NA) plates. The antibacterial activities of aerogels neat AR, AR1 and AR2 against both gram-positive and gram-negative bacteria strains were examined by detecting of the minimum inhibitory concentrations (MICs). Each sample were assayed three times and the results are shown in the figure 10 (a) and table 3. From these results,it can be observed that the antibacterial activity of AR2 is the best among all other samples (neat AR and AR2) that produced zones of inhibition against E. coli, S. typhimurium, St. aureus and B. cereus.

Determination of antioxidant activity. The antioxidant activity of the aerogels neat AR, AR1 and AR2 was evaluated using DPPH (2, 2-diphenyl-1-picrylhydrazyl from Merck, Damstadt, Germany) radical scavenging assay. Briefly, 3 mL of aerogel dispersions were mixed with 1 mL of 1mM methanolic solution of DPPH. The mixture was vortexed and incubated in the dark at ambient temperature for 30 min. When the DPPH solution was mixed with the sample mixture which is acting as a hydrogen atom donor, a stable non-radical form of DPPH is

View Article Online
DOI: 10.1039/C7NJ02392H

obtained with simultaneous change of the violet color to pale yellow. The absorbance was then measured at 517 nm. The percentage of DPPH free radical quenching activity was determined using the following equation

$$DPPH\ scavenging\ activity\% = \frac{A_{DPPH} - A_{Extract}}{A_{DPPH}} X\ 100 - - - - - - - (8)$$

where A_{DPPH} is the absorbance value at 517 nm of the methanolic solution of DPPH and $A_{Extract}$ is the absorbance value at 517 nm for the sample extract. Each sample was assayed two times and results shown in the figure 10 (b) and table 4. From this results, it can be observed that the antioxidant activity of AR2 was high compared to neat AR and AR1 as evaluated by free radical scavenging assay.

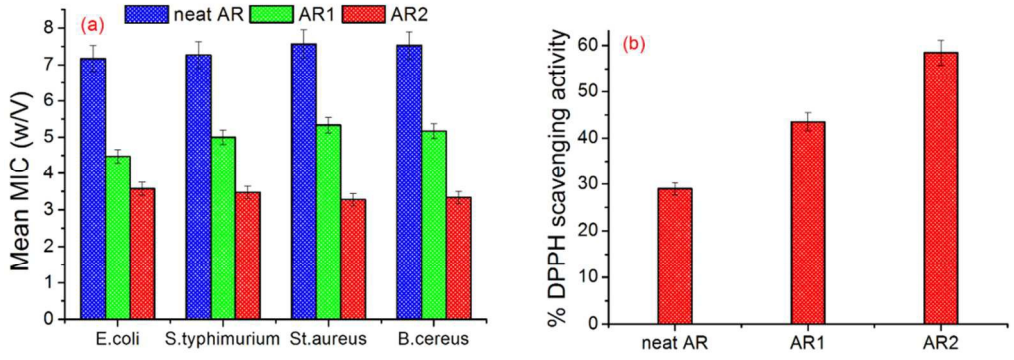

Figure 10. neat AR, AR1 and AR2 for a) antimicrobial b) antioxidant studies

Table 3. Antibacterial properties of aerogels

		MIC % (w/V)			Mean MIC % (w/V)
Sample	**Bacterial strains**	**Assay 1**	**Assay 2**	**Assay 3**	
neat AR	*E. Coli*	6.2	7.5	7.8	7.17
	S. typhimurium	6.8	7.2	7.8	7.27
	St. aureus	7.1	7.6	8	7.57
	B. cereus	6.9	7.9	7.8	7.53
AR1	*E. Coli*	5	3.8	4.6	4.47
	S. typhimurium	4.8	5	5.2	5.00

View Article Online
DOI: 10.1039/C7NJ02392H

	St. aureus	4.6	6.1	5.3	5.33
	B. cereus	5.2	4.8	5.5	5.17
AR2	*E. Coli*	3.2	4.1	3.4	3.57
	S. typhimurium	3.5	3.8	3.1	3.47
	St. aureus	3.1	3.6	3.1	3.27
	B. cereus	3.6	3.2	3.2	3.33

Table 4. Antioxidant properties of aerogels

	DPPH scavenging activity %		
Sample	**Assay 1**	**Assay 2**	**Mean DPPH scavenging activity %**
neat AR	25	33	29
AR1	41	46	43.5
AR2	55	62	58.5

The CNC embedded bio-aerogels of cellulose (mainly AR2 which contains more CNC) in which the cells stick to each other and often these cells adhere to a surface. These adherent cells are frequently embedded within a self-produced matrix of extracellular polymeric substances (EPS). Furthermore, from all the analysis it is revealed that AR2 is showing a promising result of antibacterial and antioxidant properties compared to neat AR and AR1 which may be due to the presence of acetamide group in chitin. Hence it would be interesting to investigate the potentiality of this aerogel for possible applications in different fields.

4. Conclusion

A facile green method was used to fabriacte multi-functional bio-hybrid aerogel based on CNF decorated with CNC. The morphology and propoiertis of the new nanostrucutred hybrids were charcterised using TEM, FESEM, DSC and FTIR. The chemical moeties of CNF, CNC and AR2 were analysed using FTIR spectroscopy and confirmed the presence of CNC on CNF aerogel. The CNF fibers showed wire like morphology having 60-120 nm in diameter while the CNC showed semi-square morphology having 20-100 nm in size. This semi-square morphology

View Article Online
DOI: 10.1039/C7NJ02392H

for CNC has been reported for the first time as compared to other studies in the literature. Subsequently bio-hybrid aerogels are made with different percentage of CNC (1 % and 2 %) decorted on to CNF using environmentaly friendly freeze drying method. Their morphologies were investigated with respective the reference (neat AR) and found maple like morphology for AR2. The multi functional efficiency of AR2 was evaluated using various studies such as dye water treatemnt, anti-bacterial and anti oxidant studies and realized that AR2 is a promising aerogel material for the above mentioned applications. Further studies to be anticipated in the future for industrial scale applications.

Aknowledgement

This project has received funding from the European Union's Erasmus Mundus programme, EUPHRATES, Lot 13.Sreerag Gopi is thankful to International and Inter University Centre for Nanoscience and Nanotechnology (IIUCNN), Mahatma Gandhi University and Department of Science and Technology for the support of TEM (DST Nanomission project).

References

1 A. Said A. Samir, A. F. Alloin and A. Dufresne, *Biomacromolecules*, 2005, **6**, 612–626.

2 J. Li, J.-F. Revol and R. H. Marchessault, *J. Appl. Polym. Sci.*, 1997, **65**, 373–380.

3 M. N. . Ravi Kumar, *React. Funct. Polym.*, 2000, **46**, 1–27.

4 M. Rinaudo, *Prog. Polym. Sci.*, 2006, **31**, 603–632.

5 P. M. Visakh and S. Thomas, *Waste and Biomass Valorization*, 2010, **1**, 121–134.

6 T. Lertwattanaseri, N. Ichikawa, T. Mizoguchi, Y. Tanaka and S. Chirachanchai, *Carbohydr. Res.*, 2009, **344**, 331–335.

View Article Online
DOI: 10.1039/C7NJ02392H

7 S. Ifuku, M. Nogi, K. Abe, M. Yoshioka, M. Morimoto, H. Saimoto and H. Yano, *Biomacromolecules*, 2009, **10**, 1584–1588.

8 J. F. Revol and R. H. Marchessault, *Int. J. Biol. Macromol.*, 1993, **15**, 329–35.

9 Y. Lu, L. Weng and L. Zhang, *Biomacromolecules*, 2004, **5**, 1046–1051.

10 A. Morin and A. Dufresne, *Macromolecules*, 2002, **35**, 2190–2199.

11 M. V. Tzoumaki, T. Moschakis, V. Kiosseoglou and C. G. Biliaderis, *Food Hydrocoll.*, 2011, **25**, 1521–1529.

12 J. D. G. and and W. T. Winter, *Biomacromolecules*, 2006, **8**, 252–257.

13 J. Sriupayo, P. Supaphol, J. Blackwell and R. Rujiravanit, *Carbohydr. Polym.*, 2005, **62**, 130–136.

14 E. Belamie, P. Davidson and M. M. Giraud-Guille,*J. Phys. Chem. B*, 2004, **108**, 14991–15000.

15 K. Gopalan Nair and A. Dufresne, *Biomacromolecules*, 2003, **4**, 657–665.

16 J. Junkasem, R. Rujiravanit and P. Supaphol, *Nanotechnology*, 2006, **17**, 4519–4528.

17 R. H. Marchessault, F. F. Morehead and N. M. Walter, *Nature*, 1959, **184**, 632–633.

18 S. Ifuku, M. Nogi, M. Yoshioka, M. Morimoto, H. Yano and H. Saimoto, *Carbohydr. Polym.*, 2010, **81**, 134–139.

19 B. M. Min, S. W. Lee, J. N. Lim, Y. You, T. S. Lee, P. H. Kang and W. H. Park, *Polymer (Guildf).*, 2004, **45**, 7137–7142.

20 J.-I. Kadokawa, *Green Sustain. Chem.*, 2013, **3**, 19–25.

View Article Online
DOI: 10.1039/C7NJ02392H

21 Y. Fan, T. Saito and A. Isogai, *Biomacromolecules*, 2008, **9**, 1919–1923.

22 Y. Fan, T. Saito and A. Isogai, *Carbohydr. Polym.*, 2010, **79**, 1046–1051.

23 M. Mincea, a. Negrulescu and V. Ostafe, *Rev. Adv. Mater. Sci.*, 2012, **30**, 225–242.

24 N. Lin, S. Zhao, L. Gan, P. R. Chang, T. Xia and J. Huang, *Carbohydr. Polym.*, 2017, **173**, 610–618.

25 M. A. Shannon, P. W. Bohn, M. Elimelech, J. G. Georgiadis, B. J. Mariñas and A. M. Mayes, *Nature*, 2008, **452**, 301–310.

26 J. Yuan, X. Liu, O. Akbulut, J. Hu, S. L. Suib, J. Kong and F. Stellacci, *Nat. Nanotechnol.*, 2008, **3**, 332–336.

27 G. Mezohegyi, F. P. van der Zee, J. Font, A. Fortuny and A. Fabregat, *J. Environ. Manage.*, 2012, **102**, 148–64.

28 C. H. Chan, C. H. Chia, S. Zakaria, M. S. Sajab and S. X. Chin, *RSC Adv.*, 2015, **5**, 18204–18212.

29 A. S. Bhatt, P. L. Sakaria, M. Vasudevan, R. R. Pawar, N. Sudheesh, H. C. Bajaj and H. M. Mody, *RSC Adv.*, 2012, **2**, 8663.

30 J. Ding, B. Li, Y. Liu, X. Yan, S. Zeng, X. Zhang, L. Hou, Q. Cai and J. Zhang, *J. Mater. Chem. A*, 2015, **3**, 832–839.

31 R. Xiong, C. Lu, Y. Wang, Z. Zhou, X. Zhang, X. Sun, L. Zhao, R. Zbořil and X. Zhang, *J. Mater. Chem. A*, 2013, **1**, 14910.

32 Z. Zhou, X. Zhang, C. Lu, L. Lan, G. Yuan, M. Mosiewicki, N. Marcovich and M.

View Article Online
DOI: 10.1039/C7NJ02392H

Aranguren, *RSC Adv.*, 2014, **4**, 8966.

33 H. Tamon, H. Ishizaka, T. Yamamoto and T. Suzuki, *Carbon N. Y.*, 2000, **38**, 1099–1105.

34 Q. Zheng, Z. Cai and S. Gong, *J. Mater. Chem. A*, 2014, **2**, 3110.

35 D. Klemm, F. Kramer, S. Moritz, T. Lindström, M. Ankerfors, D. Gray and A. Dorris, *Angew. Chemie Int. Ed.*, 2011, **50**, 5438–5466.

36 R. J. Moon, A. Martini, J. Nairn, J. Simonsen and J. Youngblood, *Chem. Soc. Rev.*, 2011, **40**, 3941.

37 T. Saito, M. Hirota, N. Tamura, S. Kimura, H. Fukuzumi, L. Heux and A. Isogai, *Biomacromolecules*, 2009, **10**, 1992–1996.

38 D. O. Carlsson, G. Nyström, Q. Zhou, L. A. Berglund, L. Nyholm and M. Strømme, *J. Mater. Chem.*, 2012, **22**, 19014.

39 M. Pääkkö, M. Ankerfors, H. Kosonen, A. Nykänen, S. Ahola, M. Österberg, J. Ruokolainen, J. Laine, P. T. Larsson, and O. Ikkala and T. Lindström, *Biomacromolecules*, 2007, **8**, 1934–1941.

40 M. Henriksson, G. Henriksson, L. A. Berglund and T. Lindström, *Eur. Polym. J.*, 2007, **43**, 3434–3441.

41 H. Sehaqui, M. Salajková, Q. Zhou and L. A. Berglund, *Soft Matter*, 2010, **6**, 1824.

42 W. Chen, H. Yu, Q. Li, Y. Liu and J. Li, *Soft Matter*, 2011, **7**, 10360.

43 M. Pääkkö, J. Vapaavuori, R. Silvennoinen, H. Kosonen, M. Ankerfors, T. Lindström, L. A. Berglund and O. Ikkala, *Soft Matter*, 2008, **4**, 2492.

View Article Online
DOI: 10.1039/C7NJ02392H

44 I. Díez, P. Eronen, M. Österberg, M. B. Linder, O. Ikkala and R. H. A. Ras, *Macromol. Biosci.*, 2011, **11**, 1185–1191.

45 M. Kettunen, R. J. Silvennoinen, N. Houbenov, A. Nykänen, J. Ruokolainen, J. Sainio, V. Pore, M. Kemell, M. Ankerfors, T. Lindström, M. Ritala, R. H. A. Ras and O. Ikkala, *Adv. Funct. Mater.*, 2011, **21**, 510–517.

46 J. T. Korhonen, M. Kettunen, R. H. A. Ras and O. Ikkala, *ACS Appl. Mater. Interfaces*, 2011, **3**, 1813–1816.

47 P. Khawas, A. J. Das and S. C. Deka, *Ind. Crops Prod.*, 2016, **86**, 102–112.

48 S. T. Sreerag Gopi, Anitha Pius, *J. Water Process Eng.*, 2016.

49 S. Zhu, S. Jiao, Z. Liu, G. Pang and S. Feng, *Environ. Sci. Nano*, 2014, **1**, 172.

50 X. Sun, B. Peng, Y. Ji, J. Chen and D. Li, *AIChE J.*, 2009, **55**, 2062–2069.

51 A. Krishnan K, C. Jose, K. R. Rohith and K. E. George, *Ind. Crops Prod.*, 2015, **71**, 173–184.

52 B. Wang, J. Li, J. Zhang, H. Li, P. Chen, Q. Gu and Z. Wang, *Carbohydr. Polym.*, 2013, **95**, 100–106.

53 B. Wunderlich, *Prog. Polym. Sci.*, 2003, **28**, 383–450.

54 M. Bhattacharya and A. K. Bhowmick, *J. Mater. Sci.*, 2010, **45**, 6126–6138.

55 H. Varghese, S. S. Bhagawan and S. Thomas, *J. Appl. Polym. Sci.*, 1999, **71**, 2335–2364.

56 H. Tang, C. Chang and L. Zhang, *Chem. Eng. J.*, 2011, **173**, 689–697.

57 A. Takegawa, M. aki Murakami, Y. Kaneko and J. ichi Kadokawa, *Carbohydr. Polym.*,

View Article Online
DOI: 10.1039/C7NJ02392H

2010, **79**, 85–90.

58 T. Jiao, Y. Liu, Y. Wu, Q. Zhang, X. Yan, F. Gao, A. J. P. Bauer, J. Liu, T. Zeng and B. Li, *Sci. Rep.*, 2015, **5**, 12451.

View Article Online
DOI: 10.1039/C7NJ02392H

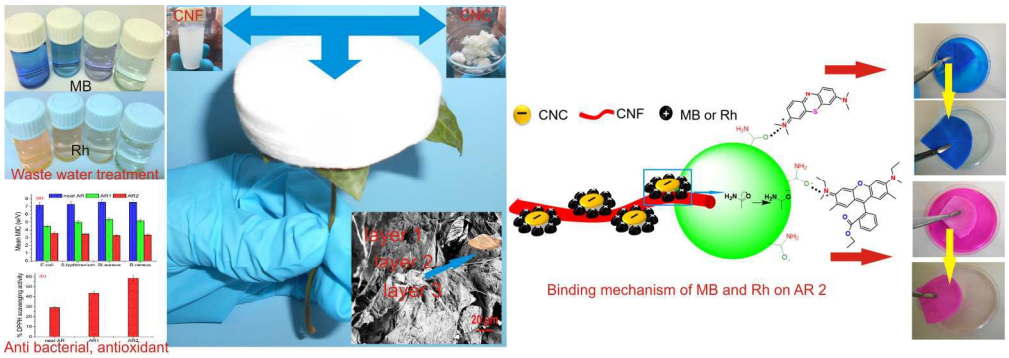

383x133mm (150 x 150 DPI)